Research Article

SOHAG JOURNAL OF SCIENCES

https://doi.org/10.21608/sjsci.2024.279081.1191

Reservoir Characteristics of Ha'py-2 well in Ha'py Gas Field, Eastern Mediterranean Region, Egypt

Abdelbaset M. Abudeif[*,1], Ahmed E. Radwan[2], Mohammed A. Mohammed[1] and Amira A. Ali[1]

[1] *Geology Department, Faculty of Science, Sohag University, Sohag82524, Egypt.*
[2] *Faculty of Geography and Geology, Institute of Geological Sciences, (Uniwersytet Jagielloński) Jagiellonian University in Krakow, Poland.*
[*]*Email: a.abudeif@science.sohag.edu.eg*

Received: 1st April 2024, **Revised:** 21st May 2024, **Accepted:** 11st June 2024
Published online: 29th July 2024

Abstract: The new discoveries recorded within the Nile Delta province throw light on the need to explore more, which encouraged using integrated studies to evaluate the petroleum systems in the offshore eastern Mediterranean area. The purpose of this study is characterizing the stratigraphic patterns, evaluating the reservoir features and identifying the depositional elements of reservoir sediments (Upper Pliocene Kafr El Sheikh Fomation) in Hap'y-2 well, Ha'py Field, eastern offshore region of the Nile Delta, Egypt. These objectives were realized using the analysis of core data, wireline logs and composite log. The results showed that the primary sand reservoir in the Hap'y-2 well is unconsolidated and the predominant control on reservoir quality is detrital clay content. The results of integrating well data analysis and core data indicate that A20 reservoir sand is an excellent example of a wave-dominated delta with a significant river effect. The extensive river input sediments are delivered to the sea, which reworks the majority of the sediments and a spit barrier system. The upper A20 unit is a shallow marine environment sand bar or shore face elongated sand bar complex. Subsurface data show that Hap'y-2 well contains at least two stacked sand bars (mounds).
Keywords: Ha'py Field; A20 Reservoir; Petrophysics; Eastern Mediterranean; Egypt.

1. Introduction

More recently, Egypt's demand for oil and gas has led to an increase in petroleum exploration. Egypt has a long history of producing and exploring hydrocarbons, making it a major producer of gas and oil. In addition to significant oil and gas discoveries in the Gulf of Suez, the Western Desert and the Nile Delta, other prospective exploration blocks were identified in the Eastern Mediterranean region, likewise a successful gas discovery in Zohr Field by Eni Petroleum Company in 2015. These discoveries shed light on offshore exploration in the Eastern Mediterranean region.

It is acknowledged that one of Egypt's most significant gas provinces is the Nile Delta region, as its sedimentary sequence indicates significant gas potential. Over 126 fields in the Nile Cone make up the approximately 223 trillion cubic feet of gas reserves that make up the Nile Delta Basin [1]. These fields were primarily created by a sizable biogenic gas source and mature source rocks from the Neogene deltaic succession [2].

Exploration drilling in the Nile Delta has increased significantly in recent years. The highly successful Pliocene play trend has been the focus of a large portion of recent drilling. In general, discovering new plays in the Pliocene portion of the Nile Delta Basin is not difficult, as the Pliocene systems are the shallowest prospects in the basin. The success rate is increased to approximately 90% because to the clear direct hydrocarbon indications (bright, flat patches) on seismic profiles those identify the shallow Pliocene gas deposits in the Nile Delta Basin [3,4].

Among the greatest fields found during the Pliocene age is Ha'py Field; it features a somewhat more complicated trapping configuration. The Plio-Pleistocene primary reservoir Hap'y Field (A20 sand) is a package of sands deposited by shallow marine. Ha'py Field is located in the eastern offshore region of the Nile Delta, Egypt, in 80m of water. It is located in the northeastern part of Ras El Barr Concession (approximately 40 kilometers from Ras El Barr Point). It is bounded by latitudes 31˚ 55'N and longitudes 31˚ 51'E (Fig. 1). The field is contained in a tilted fault-block between two N-dipping listric growth faults, which converge at the western end of the field, providing a lateral seal. The field is dip-closed to the east.

The study aims to identify the depositional elements and reservoir characteristics in the Hap'y-2 well by using different types of data, including well logs, core data and pressure data. In order to gain a deeper comprehension of the reservoir's physical characteristics and to create new avenues for exploration and development, assess the hydrocarbon potential in the area using both petrophysical and rock physics studies. As a result of this reservoir study, prospect maps were created for determining the promising and encouraging blocks for reservoir development and well recommendation plan. Location of Hap'y-2 well is shown in (Fig. 1).

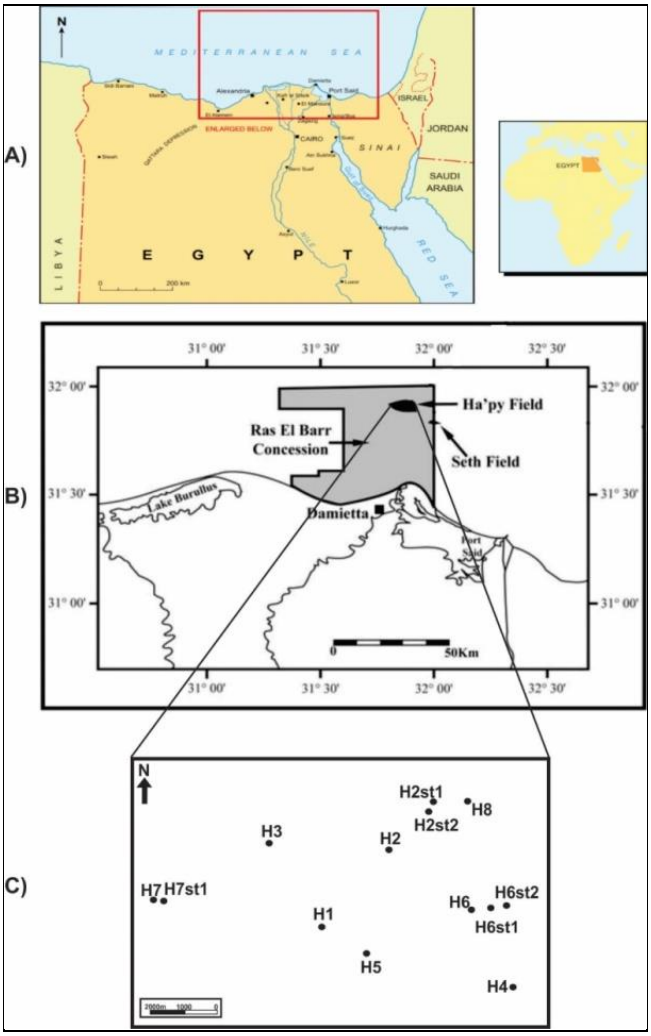

Figure 1: (**A**) Index map of the Nile Delta, Egypt. (**B**) A map showing the location of Ras El Bar concession and general layout of the Seth and Ha'py fields [5]. (**C**) location base map of Ha'py Field wells, including Hap'y-2 well [6].

2. Geologic Setting

The Nile Delta Basin covers around 250,000km² in the eastern Mediterranean [1]. Its boundaries are as follows: to the west, the margin of the Nile Cone; to the east, the Levant Basin; to the south, the boundary of the northern Egyptian compressional structures (Fig. 2); and to the north, the Pytheus, Strabo and Cyprus Trenches [1,7,8]. The Nile Delta is a sedimentary basin where the stratigraphic fill has been influenced by various external tectonic events. Two high trends divided the eastern, central and western sub-basins of the offshore Nile Delta basin (Fig. 3). Thick Plio-Pleistocene sediments coupled with a widespread shallow detachment syn-depositional listric fault system going northwest (NW) are what separate the eastern and western subbasins [9]. The study area is located within the eastern Nile Delta subbasin.

The coarse sandstone and gravel from channel sediments and the fine detrital mudstone and claystone from primarily overbank and floodplain deposits are among the many different types and thicknesses of sedimentary facies found in the stratigraphic section of the Nile Delta [10,11].

Two primary rock units, which are described below from base to top, comprised the offshore stratigraphic part of the Nile Delta [12,13]: (**A**) The sequence of sandy shale that extends from the Langhian to Messinian rock unit comprises the Moghra (sandstone), Sidi Salim (shale), Qawasim (sandstone) and Rosetta (anhydrite) formations. (**B**) The succession of shale sandstones from the Zanclean to the Holocene contains the following formations: Abu Madi (sandstone), Kafr El-Sheikh (shale), El Wastani (sandstone), MitGhamr (sandstone shale interbedded) and Bilqas (shale with sand lenses).

The Ha'py Field reserves are contained in Pliocene Kafr El Sheikh Formation sands (Fig. 4) that overlie Messinian unconformity [14]. Close to the present coast, the formation reaches its maximum thickness of roughly 2000 meters. The formation's thickness reaches approximately 1800 meters offshore to the northeast (NE) and 1500 meters near Ha'py Field. The formation is composed of a sequence of sands numbered A10 to A70 from top to bottom. Since the field's discovery, the lower part of A20 sand has been determined to be a distinct stratigraphic unit, known as A22. The A20/A22 sands contain the majority of Ha'py's reserves, with minor amounts discovered in the deeper A30 sands. The A20 Sand was initially divided into six subunits Cores from Ha'py-2, Ha'py-4, and Akhen-1 show that the A20 and A22 reservoirs consist of six main lithofacies [14].

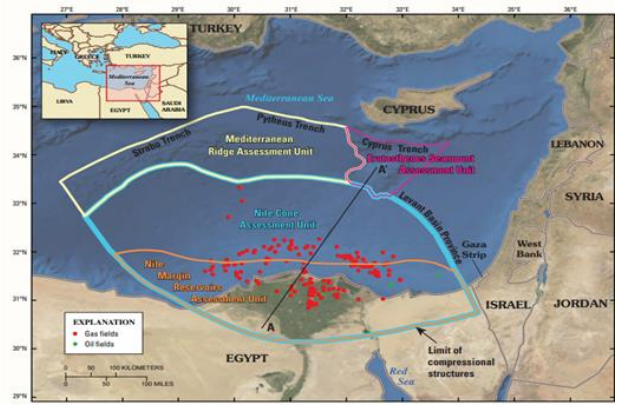

Figure 2: Four assessment units are located in the eastern Mediterranean province of the Nile Delta basin [15].

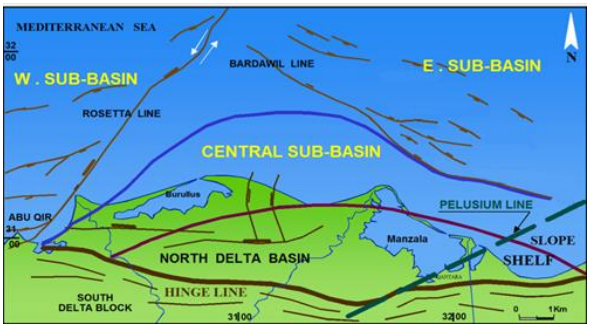

Figure 3: Nile Delta sub-surface structure pattern [9].

The reservoir sands of the Ha'py Field were initially assumed to be levee-channel turbidites and shoreline to outer shelf sediments deposited on the downthrown side of growth faults [5]. However, appraisal wells discovered a high N:G ratio, which is unusual in levee-channel deposits. Furthermore, the reservoir's seismic response did not match a levee-channel model. As a result, the prograding slump fan complex (Fig. 5) became the preferred model.

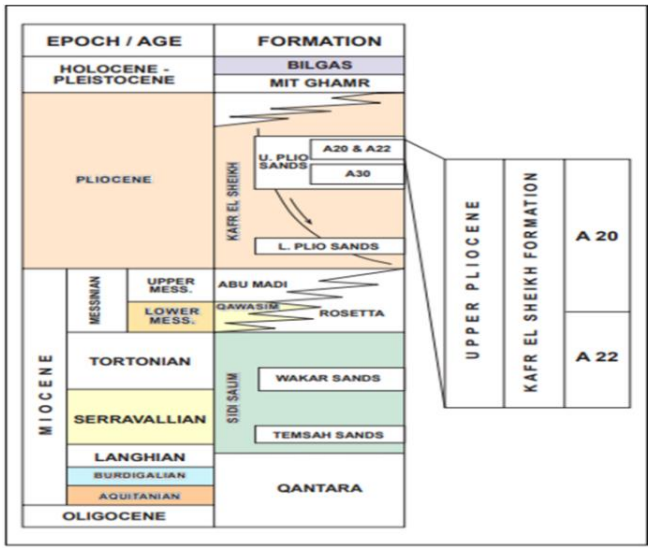

Figure 4: Stratigraphy of the Ha'py Field, whose reserves are contained in the Upper Pliocene A20/A22 and A30 sands [14].

Ha'py field accumulation is trapped between two north-dipping listric growth faults (Figs. 6 and 7) in a tilted fault-block [5,16,17]. The main reservoir is Kafr El Sheikh Formation A20/A22 Sand. The faults that provide lateral seal to the north and south strike 80 and 110, converging near the western end of the field and expanding out to the east, where the A20/A22 reservoir is dip-closed. The top seals are Kafr El Sheikh Formation shales and their sealing capacity has been shown to be extremely efficient [18].

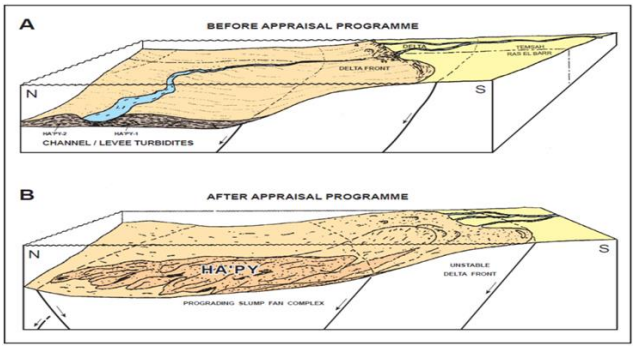

Figure 5: Depositional model for the A20 sand before (**A**) and after (**B**) the appraisal drilling program [16].

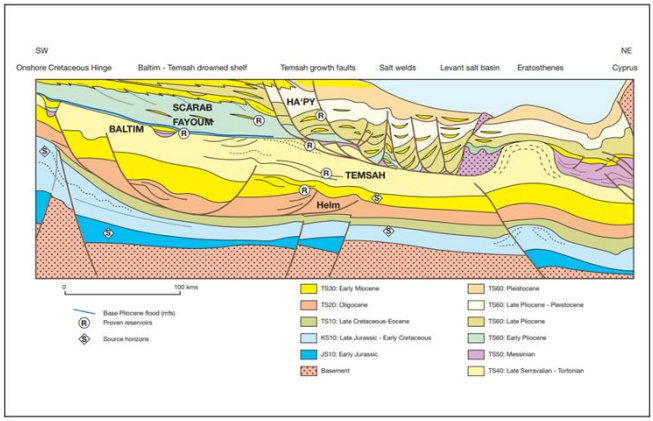

Figure 6: Regional and stratigraphic context of Ha'py Field [19]. Schematic cross-section through Nile Delta province.

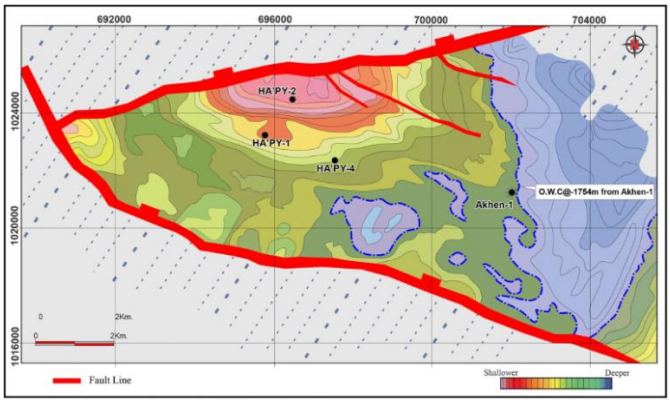

Figure 7: Structural map of Ha'py Field [17].

3. Petrography

Understanding the properties of the reservoir and the changes in log response within the analyzed zones is made easier with the aid of the formation assessment analysis, which heavily relies on the reservoir's thorough petrographic description. Petrographic studies and the identification of Ha'py sandstone reservoir quality in the studied well (Ha'py-2 well) had been made using the core samples, thin sections and XRD.

The sandstone characteristics in Ha'py-2 sandstone reservoir were described and then thin sections were used to give more details about the porosity, cementation and mineral composition of the reservoir. The thin section was made from the hard sandstones collected from the studied well and the various contents were identified under the microscope. Following that, these were integrated with the petrophysical analysis of particular well electrical logs.

The A20 and A22 reservoirs, as seen in core from Ha'py-2, Ha'py-4 and Akhen-1, comprise six main lithofacies [14]: (**1**) poorly consolidated, massive (slumped, fluidized and bioturbated), shaly sandstone; (**2**) very poorly to poorly consolidated, parallel-laminated sandstone; (**3**) very poorly consolidated, faintly laminated, shaly sandstone (often with evidence of soft sediment deformation and slumping); (**4**) poorly consolidated shaly sandstone; (**5**) well-consolidated siltstone and silty to sandy shale; and (**6**) concretionary, calcite-cemented sandstone containing bioclasts.

Petrographic analyses in Ha'py-2 well were undertaken on a total of sixty-four thin sections. Important petrographic and diagentic features are illustrated in a series of petrographic photomicrographs. This study will present some of these plates.

Petrographically, the analyzed samples comprise the following rock types: Subfeldspathic Wacke, Feldspathic Wacke, Subfeldspathic Arenite, Feldspathic Arenite and Quartz Wacke.

The majority of samples are enriched in quartz, feldspars, detrital clays, lithics and, in some cases, glaucony and bioclasts, with subordinate quantities of mica, carbonaceous debris and rare phosphatic fragments. Feldspars, lithics, bioclasts and glaucony grain types are significantly leached during late-stage diagenesis, indicating that the original composition of these samples contained more feldspars, lithics and other labile grains. The ratio of Quartz: Feldspar: Lithic for all samples is 76.8:21.5:1.7. This ratio suggests that the sandstones are often immature to submature in terms of mineralogy.

Generally, all samples are poorly compacted. Grains show point grain contact with local subordinate long grain contacts. Grain sizes range from the lower limit of very fine sand (vfL) to the upper limit of medium sand (mU) grade, with an average grain size range from the lower limit of fine sand (fL) to the upper limit of fine sand (fU). In general, the sandstone samples are moderate-well to very well sorted. There are two types of grain roundness: subangular and subrounded. The degree of roundness, particularly for the quartz grains, is modified by grain etching. Pore types are dominated by primary and secondary interparticle forms, although the removal of feldspars, glaucony, lithics, bioclasts and dolomite cement created secondary intraparticle pores. Most of the samples are clay-rich sandstones (Wacke) with a significant amount of microporosity.

The average pore size of all samples varies from 10 microns to 100–200 microns. Pore interconnectivity ranges from poor-moderate to good. Point-counted porosities vary from 2% to 21%, whereas for the same samples, helium porosities range from 13.2% to 37.9%. The increase in helium porosity values compared to point counted porosity in all samples is related to microporosity within different detrital and authigenic clay phases. Some of core samples in Ha'py-2 well at different depths are illustrated in (Fig. **8**). In this study, three plates (Plates A, B and C) will be presented as thin sections and their descriptions in Ha'py-2 well as following:

- **Plate A (2037.55m)**

The rock type in this plate (Fig. **9**) is Feldspathic wacke, fine lower grained, well sorted and poorly compacted. The detrital grains are dominantly monocrystalline quartz grains, potassium feldspars, plagioclase feldspars, oxidized glaucony pellets and minor bioclastic debris, the detrital clays are abundant grain coating and pore filling dispersed detrital clays, the cement is rare aggregates of pyrite, chloritized glaucony and illitized detrital clays. The pore network is moderately interconnected pore system. Porosity is dominated by interparticle pores and secondary intraparticle dissolution porosity (feldspars and glaucony). Significant microporosity occurred within various clay types. The reservoir quality in this plate is moderate with porosity of 6%.

- **Plate B (2038.10m)**

The rock type in this plate (Fig. **10**) is Glauconitic feldspathic wacke, fine lower grained, well sorted and poorly to moderately compacted. The detrital grains are abundant monocrystalline quartz grains, polycrystalline quartz, potassium feldspars, plagioclase feldspars, oxidized glaucony pellets and minor bioclastic debris (molluscs). Minor carbonaceous matter, the detrital clays are common grain coating and pore filling dispersed detrital clays, the cement is minor subcubic pyrite crystals, rare chloritized glaucony and illitized detrital clays. The pore network is moderately interconnected pore system. Porosity is dominated by interparticle pores and secondary intraparticle dissolution porosity (feldspars and glaucony). Significant microporosity occurred within different types of clay. The reservoir quality in this plate is moderate to good with porosity of 8%.

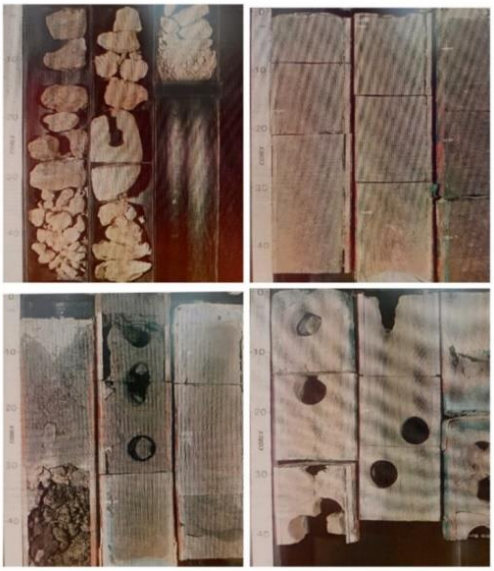

Figure 8: Core samples in Ha'py-2 well at different depths.

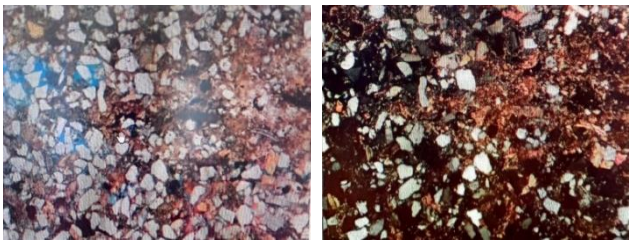

Figure 9: Photomicrograph of thin section sample at depth 2037.55m (plate **A**), Ha'py-2 well.

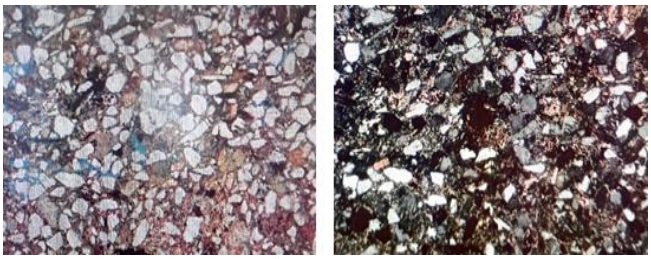

Figure 10: Photomicrograph of thin section sample at depth 2038.10m (plate **B**), Ha'py-2 well.

- **Plate C (2038.50m)**

The rock type in this plate (Fig. **11**) is Subfeldspathic wacke, fine lower grained, well sorted and poorly compacted. The detrital grains aredominantly monocrystalline quartz grains, polycrystalline quartz, chert fragments, potassium feldspars, plagioclase feldspars, oxidized glaucony pellets and bioclastic debris (algae, molluscs). Minor carbonaceous matter, the detrital clays are abundant grain coating and pore filling dispersed detrital clays, the cement is rare aggregates of pyrite, chloritized glaucony and illitized detrital clays. The pore network is moderately interconnected pore system. Porosity is dominated by interparticle pores and secondary intraparticle dissolution porosity (feldspars, glaucony and bioclasts). Significant microporosity occurred within different types of clay. The reservoir quality in this plate is moderate to good with porosity of 13%.

Figure 11: Photomicrograph of thin section sample at depth 2038.50m (plate C), Ha'py-2 well.

2.1 XRD of Ha'py-2 well

X-ray Diffraction (XRD) is the gold standard of all mineral identification/quantification techniques. The evaluation of clay kinds and volumes that cannot be ascertained by thin section or SEM investigation is made possible by X-Ray Diffraction (XRD). Table **1** shows the X-Ray diffraction data of Ha'py-2 well at different depths (from 2010.25m to 2037.25m). These data show that:

Quartz: Monocrystalline quartz with undulose extinction is the dominant framework grain (42% to 82%) with average 69.6% in Ha'py-2 well. Polycrystalline quartz is relatively common in the coarser grained subfeldspathic arenites.

Plagioclase: Plagioclase feldspars (1% to 12% by volume) with average 5.5%, they occur in all the samples but are relatively less abundant compared to potassium feldspars and are usually fresh (unaltered) and occasionally cloudy (sericitized or illitised) or leached preferentially along cleavage planes. In some circumstances, grains can be completely dissolved, only marked by relics of earlier grain boundaries.

K-Feldspars: Detrital feldspars are recorded in all the analyzed sandstones. Potassium feldspars (trace to 13% by volume) with average 4.3%. Potassium feldspars include microcline, orthoclase and perthite. Microcline is the dominant potassium feldspar type in most of the samples of core no. 1 (samples from 2009m to 2014.5m), whereas orthoclase and perthite (stained yellow) are dominant throughout the rest of the samples. Potassium feldspars show a range in the degree of alteration, from relatively unaltered grains to leached skeletal varieties.

Dolomite: Abundant pore filling and grain replacive ferroan dolomite cements occur only in two samples: 2031m (11% by volume) and 2036.5m (29.5% by volume), the average of dolomite in Ha'py-2 well is 0.5%.

Calcite: Calcite occurs in one sample at 2017m (2.5% by volume) as a pore filling and grain replacive precipitate, the average of calcite in Ha'py-2 well is 4.7%.

Pyrite: Authigenic pyrite is a ubiquitous polyphase cementing and replacive agent ranging from trace to 2% by volume, pyrite occurs in one sample at 2032.75m. The average of pyrite in Ha'py-2 well is 0.2%.

Halite: Halite is absent in samples of Ha'py-2 well.

Clays: Clays are relatively common in most of the samples, ranging from 7 to 19% by volume with average 11.9%. Petrographic observations suggest that the vast majority of interstitial clay is of detrital origin and locally replaced by minor microcrystalline dolomite, probably illitized and rarely chloritized.

The average in Ha'py-2 well of Ankerite (2.9%), clinoptilolite (0.2%), heulandite (0.3%).

Table 1. X-Ray Diffraction Data of Ha'py-2 well, by the company of AMOCO.

Depth	Bulk Mineralogy (%)										Clay Mineralogy (%)					
	Quartz	Plagioclase	K-Feldspars	Calcite	Ankerite	Dolomite	Clinoptilolite	Heulandite	Pyrite	Halite	Total Clay	Kaolinite	Chlorite	Illite	Smectite	MXL I/S*	% Illite in MXL
Ha'py 2																	
2010.25 m	75	7	Tr	1	7	1	0	0	0	0	8	2	0	1	5	0	0
2011.25 m	70	4	8	4	0	0	0	2	0	0	12	3	0	2	7	0	0
2013.75 m	80	7	4	0	4	0	Tr	0	0	0	5	1	Tr	1	3	0	0
2016.75 m	42	7	5	26	0	1	0	0	0	0	19	6	0	4	9	0	0
2018.75 m	74	3	1	2	0	1	0	2	0	0	17	7	0	3	7	0	0
2019.75 m	82	2	4	1	0	1	0	0	0	0	10	2	1	1	6	0	0
2025 m	63	9	13	5	0	0	1	0	0	0	9	2	1	1	5	0	0
2029.75 m	77	3	2	4	5	0	0	0	0	0	9	3	0	2	4	0	0
2031.85	58	12	1	9	0	2	0	0	0	0	19	7	0	4	8	0	0
2032.75 m	68	1	10	0	5	0	0	0	2	0	15	2	1	2	10	0	0
2035.25 m	64	10	2	2	8	0	0	0	0	0	13	2	1	2	8	0	0
2037.25 m	82	1	1	2	6	0	1	0	0	0	7	1	1	1	4	0	0
Ha'py-2 Average	69.6	5.5	4.3	4.7	2.9	0.5	0.2	0.3	0.2	0.0	11.9	3.2	0.4	2.0	6.3	0.0	0.0
												26.5734	3.4965	16.7832	53.1469	0	0

XRD shows Ha'py-2 (A20) reservoir sands average clay composition as following:

Most samples contain high amounts of smectite from 3% to 10%, kaolinite comes after smectite as it ranges from 1% to 7%, low amounts of illite occurs in samples ranges from 1% to 4% and chlorite occurs in trace amounts in some samples.

Depending on the previous data, the results of XRD of samples in this zone of Ha'py-2 well show that the average percentage of clay minerals are (Fig. **12**):

Smectite (53%), kaolinite (27%), Illite (17%) and Chlorite (3%).

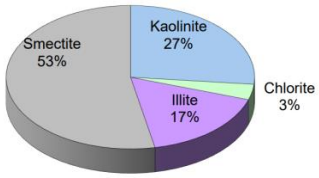

Figure 12: Ha'py-2 (A20) reservoir sands average clay composition from XRD.

4. Materials and Methods

The Pharaonic Petroleum Company graciously provided the data utilized in this investigation. The available data used in this study includes geologic reports, wells location and base maps, structure contour map, data core analysis and wire-line logs for Ha'py-2.

For this well, corrected density, resistivity, neutron, gamma ray and sonic logs are available. Additionally, available is Composite Logs, which comprise the lithologic description and the chromatograph data, both of which are helpful in identifying the zones that contain hydrocarbons.

A detailed examination was done in the Ha'py-2 well to characterize the sandstone reservoirs and a complete petrographic description was done to delineate the reservoir characteristics by using core samples and thin sections. Petrographic descriptions of these sand zones have been done using core samples and thin sections to determine the primary reservoir properties of the Ha'py field sands, such as lithology, cementation and accessory minerals, visual porosity and oil shows.

The well logging data are used to determine the petrophysical characteristics of the studied intervals using the formation evaluation system. The theory of this system is that well log analysis is based on the total use of equations and formulae, as well as pre-established charts and cross-plots for the required petrophysical parameters, particularly those

relating to lithology, water, porosity and hydrocarbon saturation using computer software. The analysis of the well log data starts with the arrangement of log data in a readable format using LAS format or an Excel spreadsheet. Log files are imported into the Techlog software package (powered by Schlumberger). The well logging analysis method included the following measurements: water resistivity (Rw), which was obtained graphically from Pickett's plot; effective porosity; formation temperature; total porosity; shale volume; and hydrocarbon and water saturation.

4.1. Shale volume determination (V_{sh})

Calculating the shale volume (Vsh) is critical for differentiating between reservoir and non-reservoir rocks. Shale volume can be calculated from density and neutron logs, as shown in equation (**1**):

$$V_{sh(ND)} = \frac{(\Phi_d - \Phi_n)}{(\Phi_{n_{sh}} - \Phi_{d_{sh}})} \text{.....(1)}$$

where: V_{sh} is the shale volume (%), Φ_d is the density porosity in sand, Φ_n is the neutron porosity in sand, $\Phi_{n_{sh}}$ is the neutron porosity in adjacent shale and $\Phi_{d_{sh}}$ is the density porosity in adjacent shale.

4.2. Formation porosity determination (Φ)

The porosity of a zone can be determined either from a single porosity log (sonic, density, neutron) or a combination of porosity logs in order to correct for varying lithology effects in complicated reservoirs.

Density logs work best for determining porosity in consolidated rocks, while neutron logs are highly successful in measuring porosity in clean, unconsolidated sands. By monitoring the time, it takes for sound waves to pass through a rock, which is correlated with both density and neutron porosity, sonic logs can be used to assess porosity.

When combined, these logs can provide a comprehensive image of the porosity and fluid storage capacity of the reservoir.

In the present study, the methods used to determine porosity are:

4.2.1. Density porosity (Φ_D)

The formation density log is a porosity log that determines the electron density of a formation. The density porosity can be determined by using the following equation (**2**):

$$\Phi_D = \frac{\rho_{mat} - \rho_b}{\rho_{mat} - \rho_f} \text{ ..... (2)}$$

where: Φ_D is the porosity from density log (%), ρ_{mat} is the matrix density (gm/cc), ρ_b is the bulk density (gm/cc) and ρ_f is the fluid density (gm/cc).

4.2.2. Neutron porosity (Φ_N)

The neutron method responds to the presence of hydrogen. In clean formations, where pores are filled with oil or water, the neutron log determines liquid-filled porosity.

When pores are filled with gas instead of oil or water, the measured neutron porosity is lower than the actual formation porosity; this decrease in neutron porosity caused by gas presence is called the gas effect.

When clays are present in the formation matrix, the measured neutron porosity is greater than the actual formation porosity; this increase in neutron porosity caused by the presence of clays is called the shale effect.

Consequently, the neutron porosity must be corrected using equation (**3**) [20]:

$$\Phi_N = \Phi_{log} - V_{sh}\,\Phi_{sh} \text{ ..... (3)}$$

where: Φ_N is the porosity from neutron log (%), Φ_{log} is the apparent neutron porosity reading on the log, Φ_{sh} is the neutron porosity of shale and V_{sh} is the volume of shale.

4.2.3. Neutron-Density porosity ($\Phi_{N\text{-}D}$)

The combination of neutron and density measurements may be the most commonly used porosity log combination. Gas in the pores increases density porosity (which is lower than oil or water) and decreases neutron porosity. In that zone, neutron porosity is lower than density porosity and the two porosity curves cross over each other.

The effect of gas on the Neutron-Density log is a very important log response because it helps a geologist to detect gas-bearing zones.

In the study area, combining the neutron and density porosities was the best one for calculating porosity in the reservoir. The crossover is found and the width of the cross-over changes according to the saturation percentages and shale content. The high width of cross-over is because of the gas-bearing sand effect and the low width is either the water effect or the shaly water effect.

Equation (**4**) is used to determine the neutron-density porosity for gas bearing formtion.

$$\Phi_{N\text{-}D} = \sqrt{\frac{\Phi_N^2 + \Phi_D^2}{2}} \text{ ..... (4)}$$

where: ($\Phi_{N\text{-}D}$) is the neutron-density porosity, (Φ_N) is the neutron porosity and (Φ_D) is the density porosity.

4.2.4. Determination of total porosity (Φ_t)

Porosity measurements with neutron-density combinations provide an estimate of total porosity (Φ_t), which is all the pore space in the reservoir, whether the pores are interconnected or isolated.

4.2.5. Determination of effective porosity (Φe)

Effective porosity refers to the amount of connected void space that can transfer fluids.

Before applying effective porosity equation, the density and neutron porosities are first corrected for the shaliness effect on porosity. Equation (**5**) is used to determine effective porosity:

$$\Phi_{eff} = \Phi_t - (V_{sh} * \Phi_{sh}) \text{ ..... (5)}$$

where: (Φ_{eff}) is the effective porosity, (Φ_t) is the total porosity from neutron or any method, (V_{sh}) is the Volume of shale from non-linear equation or any and (Φ_{sh}) is the neutron porosity reading in 100% shale or clay.

4.3. Water Resistivity estimation (R_W)

In certain reservoirs, freshwater intrusion, temperature changes, salinity and shifting depositional environments can all have a substantial impact on the value of R_w from well to well [21]. Practically, there are various ways to estimate the formation water resistivity (R_w) such as the following methods:

4.3.1. Archie's Formula

Archie formula has been commonly used by many log analysts particularly when dealing with clean sand reservoirs. In saturated rocks, there is a correlation between porosity and the formation resistivity factor (F_R). Equation (**6**) was proposed by [22] for clean granular rock that is not argillaceous.

$$F_R = \frac{Ro}{Rw} \text{.....(6)}$$

where: (F_R) is the formation resistivity factor, (R_0) is the resistivity of a formation 100% saturated with formation water and (R_w) is the formation water resistivity.

In this work, the previous method has not been applied.

4.3.2. Pickett Plot

The Pickett plot [23,24] is one of the most common and effective crossplot methods in use. In addition to estimating water saturation, the method can be used to calculate cementation factor (m) and formation water resistivity (R_w). The Pickett technique relies on the finding that porosity (Φ), water saturation (S_w), and cementation exponent (m) all affect true resistivity (R_t). In actuality, it is a graphical solution to resistivity-based Archie's equation; equation (**7**).

$$\log R_t = \log (aR_w) - m \log \Phi \text{.....(7)}$$

This form of the equation (y=b+mx) shows that by plotting R_t on the y-axis against porosity (Φ) on the x-axis (on a logarithmic scale), the product ($a*R_w$) can be calculated from the line's intercept (b) and the cementation exponent (m) from the slope of the line (m).

4.4. Water Saturation determination (S_w)

Water saturation (S_w) is the primary petrophysical property that is utilized to identify a unique reservoir [25]. While there are a number of formulae available for calculating water saturation, Archie's Indonesian equation; equation (**8**) is the most widely used and crucial one.

$$S_w = \left\{ \frac{\sqrt{\frac{1}{Rt}}}{\left(\frac{Vsh^{(1-0.5Vsh)}}{\sqrt{Rsh}}\right) + \sqrt{\frac{\Phi^m}{aRw}}} \right\}^{(2/n)} \text{.....(8)}$$

where: S_w is the water saturation, R_{sh} is the resistivity of a thick shale unit, R_t is the true resistivity of the uninvaded formation, V_{sh} is the volume of shale, Φ is the porosity, R_w is the resistivity of formation water and m is the cementation factor.

4.5. Permeability determination (K)

The ease of fluid movement inside a rock body is referred to as permeability. Although it doesn't necessarily rely on porosity, it is connected to it.

The permeability is determined by using Coates equation (**9**) [26]; water saturation that is more than the free water level is regarded as irreducible.

$$K = K_c \times \Phi_{eff}^4 \times \left(\frac{1-Swirr}{Swirr}\right)^2 \text{ ..... (9)}$$

where: (S_{wirr})=irreducible water saturation, (Φ_{eff})=effective porosity, and (k_c)=permeability coefficient (default value used in techlog software is 650).

The irreducible water saturation can be calculated using the following equation (**10**):

$$S_{wirr} = \frac{BVW}{\Phi} \text{.....(10)}$$

where: (S_{wirr}) is irreducible water saturation, (BVW) is bulk volume water and (Φ) is porosity from Neutron Density.

4.6. Gas saturation determination (Sg)

Equation (**8**) utilized effective porosity to compute water saturation and in turn Equation (**11**) was used to compute hydrocarbon (gas) saturation.

$$S_g = (1 - S_w) \text{ ..... (11)}$$

where: (S_g) is the hydrocarbon (gas) saturation and (S_w) is the water saturation.

4.7. Lithology identification and interpretation

The Neutron-Density Crossplot technique helps geologists with lithologic determination and mapping. When lithologic data from cores or samples is not available, this method becomes very crucial for geologists [27].

4.7.1. Neutron-Density Crossplot

Neutron-density crossplots are commonly employed to precisely compute the matrix porosity in carbonate rocks and determine the lithology (using the neutron and density logs). Here, the neutron porosity (NPHI) and bulk density (RHOB) measurements are displayed together.

Quartz sandstones, dolomites and calcites (limestones) are the common reservoir rocks that may be distinguished from one another using neutron density. In addition, it can be used for identification of shales and some evaporates. It also can help in gas detection.

4.8. Netpay thickness determination

Utilizing the Techlog program, the Netpay thickness is calculated by averaging the pay net flag.

5. Results and Discussion

The petrophysical evaluation of the Kafr El Sheikh Formation in the research region includes the investigation of several petrophysical parameters, such as porosity, water saturation, permeability, shale content and hydrocarbon saturation based on wireline logging data. Ha'py-2 well logging data was used in these analyses.

5.1. Petrophysical interpretation log analysis of Ha'py-2 well

Lithology Analysis: Shale and sandstone formations are included in the Ha'py-2 well's lithological composition (Fig. 13), which was determined using neutron-densit and pickett plots as shown in (figs. 14 and 15). They can also be determined by using gamma-ray log data, it was possible to identify the reservoir's sandstone-dominated and shale-rich intervals.

Porosity Distribution: Porosity values are not constant, with a range of 0.28 to 0.36. The reservoir rock's varied pore spaces are reflected in this range, which enhances the rock's ability to store hydrocarbons.

Permeability Variation: The permeability values in the Ha'py-2 well range from 0.01 to 505.23 millidarcies. The wide range of permeability indicates reservoir heterogeneity, which affects fluid flow efficiency within the geological formation.

Hydrocarbon Reservoir Classification: One important factor in classifying hydrocarbon reservoirs is the effective water saturation. A zone is classified as a hydrocarbon reservoir if its effective water saturation value is less than 50% and as a non-reservoir if its value is greater than 50%. This criterion makes it easier to pinpoint areas with the right amount of hydrocarbons.

Shale Volume Influence: Classifying reservoirs is mostly dependent on the shale volume. Reservoir zones are indicated by shale volumes less than 35%, whilst non-reservoir areas are suggested by volumes greater than 35%. Identifying zones with advantageous reservoir characteristics is aided by this parameter.

Table 2. Summary table shows the petrophysical results for the promising zones within Ha'py-2 well.

Well Name	Top (TVDSS) (m)	Bottom (TVDSS) (m)	Gross reservoir thickness (m)	Net Pay Thickness (m)	N/G ratio	V_{sh} (%)	Φ_{eff} (%)	S_w (%)	Permeability (millidarcies)
Ha'py-2 (Kafr El-Sheikh Formation)	1207.743	1813.577	A20: 136 m (maximum)	136 m (maximum)	> 0.75 (commonly approaching 1)	< 20	28 – 36	10 – 60	0.01 to 505.23

The calculated petrophysical parameters for the highly promising characteristics for gas production, including low shale volume (less than 20%), high effective porosity (28-36%), low water saturation (10-60%), low bulk volume water, increase in values of effective gas permeability and the decrease in water permeability.

In conclusion, a thorough understanding of the petrophysical properties of the Ha'py-2 well is provided by the lithological study performed using gamma-ray logs in conjunction with the measurements of porosity, effective water, saturation, permeability and shale volume. These results provide valuable information for reservoir characterization and serve as a foundation for well-informed decisions about reservoir management and hydrocarbon recovery strategies.

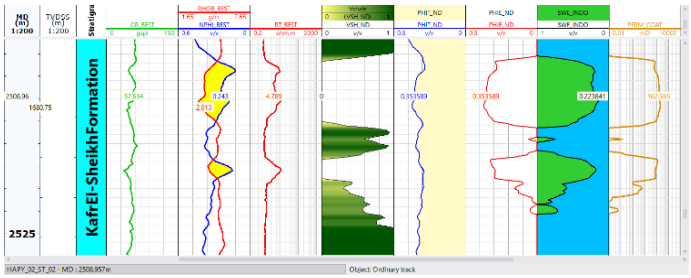

Figure 13: Petrophysical interpretation log analysis of Ha'py-2 well.

5.2. Pickett Plot of Ha'py-2 well

Points representing the gas zones in the studied well are clustered and placed below the Sw=50% line, reflecting the gas potential of these intervals and confirming the completed petrophysical calculations.

The points located around the line of Sw=25% represented low GR, high resistivity values and very low shale content. So, it's called gas bearing sandstone (Fig. **14**).

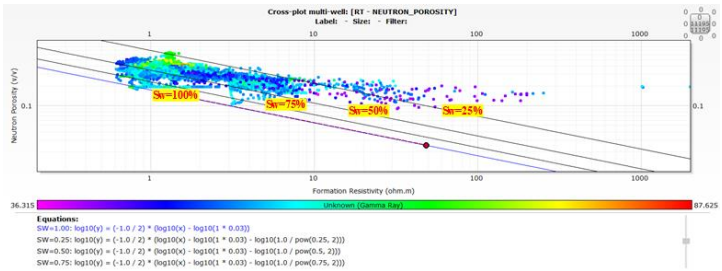

Figure 14: Pickett Plot of Ha'py-2 well.

5.3. Neutron-density Plot of Ha'py-2 well

The data points that are above the clean quartz line can be considered to have a gas effect. So, the points that flagged

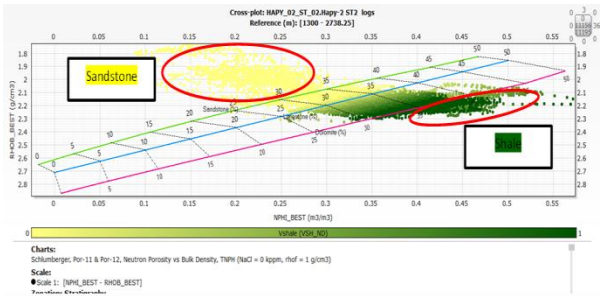

yellow and aligned to upward denote gas bearing sands with porosity ranging in values from 28 to 36%. The neutron porosity, low bulk density and low gamma ray values are all intermediate at these points (Fig. **15**).

Figure 15: Neutron-density Plot of Ha'py-2 well.

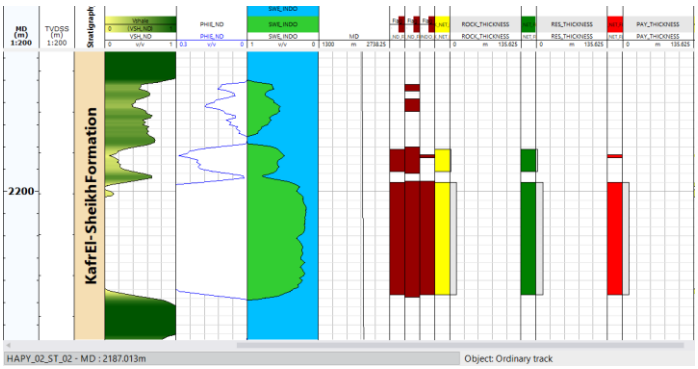

5.4. Netpay thickness

The depth to the top pay in A20 reservoir is about 1350m TVDSS (true vertical depth subsea). The Netpay thickness in this reservoir reaches to its maximum (~ 136m) in Ha'py-2 well (**Fig. 16**).

Figure 16: Cut-off of Ha'py-2 well, showing the net pay of A20 reservoir in Ha'py-2 well.

5.5. Cut-off determination

Petrophysical cutoffs are the minimum or maximum values of particular petrophysical parameters that determine reservoir zones. Petrophysical cutoffs vary depending on the reservoir type, fluid characteristics and geological setting. They can be determined by core analysis, well logs or statistical methods.

according these cutoffs there is one reservoir (A20 reservoir) in Ha'py-2 well.

There are three parameters that are used to identify reservoir zones (shale volume, porosity and water saturation).

Table 3 shows the workflow table flags for these parameters. The yellow color represents the rock flag, in which the shale content is cut off, while the green color represents the reservoir flag, in which the shale content and porosity are cut-offs and the red color represents the pay flag, in which the three parameters (shale content, porosity and water saturation) are cut-offs.

Figure 16 shows these cut-offs in Ha'py-2 well, showing the net pay of A20 reservoir in this well.

Table 3. Workflow table flags of the field cut-offs.

	Flag Name	Flag shading colour	Shale Volume cutoff	Porosity cutoff	Water Saturation cutoff
1	ROCK		yes	no	no
2	RES		yes	yes	no
3	PAY		yes	yes	yes

5.5.1 Cut-off of shale content

The shale content-effective porosity relationship between the well and the gamma ray log was used to determine the cutoff value. The shale content-porosity cross plot and gamma ray log used to determine the shale content cut-off are shown in (fig. 17). The plot shows that the volume of shale cut-off (V_{sh}) value for reservoir and non-reservoir rocks is 0.35, indicating that rocks with a shale content of less than or equal to 35% are classified as reservoir rocks, while rocks with a shale content greater than 35% are classified as non-reservoir rocks. This method is widely used to detect and distinguish sand intervals from shale [28,29].

5.5.2 Cut-off of water saturation

The effective water saturation-effective porosity cross plot and gamma ray log are commonly used to distinguish productive (pay) intervals from non-productive (non-pay) intervals in porous rocks (Fig. 18). In this case, a water saturation value that is less than 50% is utilized as the cutoff for determining pay zones, indicating that intervals with water saturation values larger than 50% are considered non-productive. This cutoff depends on the assumption that oil or gas is unlikely to be found in intervals with high water saturation levels. Even so, the efficiency of this cutoff may vary based on the geological characteristics of the reservoir under study.

5.5.3 Porosity cut-off

The porosity cutoff is an essential parameter for differentiating various sand interval types. Particularly, a minimum porosity value is necessary for the sand to be permeable enough to allow oil and gas to pass through. Porosity values of 10% or above are commonly considered sufficient for permeability and are hence used to identify reservoirs from non-reservoirs [30]. However, it is essential to keep in mind that other factors, such as the nature of the pore space, can influence permeability and must be considered when assessing a potential reservoir.

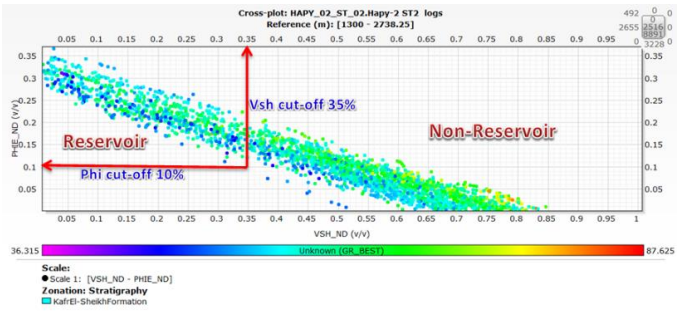

Figure 17: Shale content versus porosity crossplot and gamma ray log for cut-off determination of Ha'py-2 well.

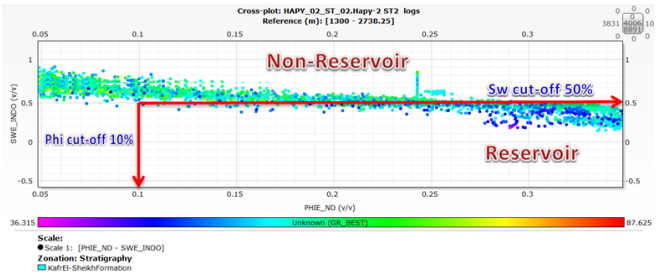

Figure 18: Porosity-water saturation cross plot for cut-off determination of Ha'py-2 well.

6. Conclusion

The reservoir sands of the Ha'py Field were initially assumed to be levee-channel turbidites and shoreline to outer shelf sediments deposited on the downthrown side of growth faults. Ha'py field accumulation is trapped between two N-dipping listric growth faults in a tilted fault-block. Lithological identification techniques confirmed that the lithology is characterized by a moderate to poorly sorted, very fine to fine-grained feldspathic to subfeldspathic arenites. The core analysis data showed that the majority of the samples are enriched in quartz, feldspars, detrital clays, lithics and, in some cases, glaucony and bioclasts, with subordinate quantities of mica, carbonaceous debris and rare phosphatic fragments.

The results of XRD of some samples in Ha'py-2 well showed that the average percentages of clay minerals are: Smectite (53%), kaolinite (27%), Illite (17%) and small amounts of Chlorite (3%).

One particularly noteworthy and extremely prospective reservoir rock found in the study well is the Kafr El Sheikh Formation. Shale contents less than or equal to 35% are categorized as reservoir rocks in the study region; samples containing more than 35% of shale are categorized as non-reservoir rocks. Identifying the sand intervals and separating them from the shale are frequently accomplished using this method.

The effective porosity levels exhibit variability from 28-36% (avg. 32%), the type of this porosity is primary intergranular. In this case, the cutoff for identifying pay zones is a water saturation value less than 50%, meaning that intervals with a water saturation value more than 50% are categorized as non-productive. The depth to top pay is A20: ~1350m TVDSS.

The maximum Netpay thickness is 136m.

Based on this study and the continuous hydrocarbon gas discoveries in the Mediterranean region. The Eastern Mediterranean region is considered one of the most promising exploration blocks, as it is expected that more discoveries will be made there in the future.

CRediT authorship contribution statement:

Conceptualization, A.M.Abudeif and A.E. Radwan.; methodology, A.A. Ali.; software, A.A. Ali .; validation, A.M. Abudeif and M.A.Mohamed; formal analysis, A.A. Ali and A.E. Radwan; investigation, A.A. Ali A.M Abudeif.; resources, A.E. Radwan; data curation, M.A.Mohamed.; writing—original draft preparation, A.A. Ali.; writing—review and editing, A.M.Abudeif.; visualization, M.A.Mohamed.; supervision, A.M.Abudeuf, M.A. Mohamed, and A.E.Radwan; project administration, No.; funding acquisition, No Funding. All authors have read and agreed to the published version of the manuscript."

Data availability statement

The data used to support the findings of this study are available from the corresponding author upon request.

Declaration of competing interest

The authors declare that they have no known competing financial interests or personal relationships that could have appeared to influence the work reported in this paper.

Acknowledgment

We express our profound gratitude to the Pharaonic Petroleum Company and the Egyptian General Petroleum Company authorities for allowing us to utilize their data for this research.

References

[1] Kirschbaum, M.A., Schenk, C.J., Charpentier, R.R., Klett, T.R., Brownfield, M.E., Pitman, J.K., Cook, T.A., and Tennyson, M.E., *U.S. Geological Survey Fact Sheet* 4 (2010) 2010-3027.

[2] Vandré, C., Cramer, B., Gerling, P., Winsemann, J., *Organic Geochemistry*, 38(4) (2007) 523-539.

[3] Dolson, J.C., Boucher, P.J., Siok, J., Heppard, P.D., *In Geological Society, London, Petroleum Geology Conference Series*, 6(1) (2005) 607-624.

[4] Samuel, A., Kneller, B., Raslan, S., Sharp, A., Parsons, C., *AAPG Bulletin*, 87(4) (2003) 541-560.

[5] Wigger, S., Simpson, M., Nada, H., Larsen, M.J., Haggag, M., *In EGPC: 13th petroleum conference*, 1 (1996) 185-193.

[6] *BP annual report database*, 2009.

[7] Roberts, G., D. Peace, *GeoArabia*, 12(3) (2007) 99-124.

[8] Robertson, A.H., *Proceedings of the Ocean Drilling Program, Scientific Results*, 160 (1998) 723-732.

[9] Hemdan, K., El Alfy, M., Enani, N., Barrasi, M., Monir, M., *Mediterranean offshore conference*, (2002) 45-56.

[10] Eysa, E.A., El Khadragy, A.A., Hashim, A., Abd El Kader, A., *IOSR J Appl Geol Geophys*, 3 (2015) 50-67.

[11] Said, R., *Rotterdam, Brookfield*, (1990) 734.

[12] Issawi, B., El-Hinnawi, M., Francis, M., Mazhar, A., *Geol. Survey Cairo*, 76 (1999) 462.

[13] *EGPC, Egyptian General Petroleum Corporation, Cairo*, (1994) 387.

[14] Freeman, P.J., and Gunter, G.W., *Proceedings 14th Petroleum Exploration & Production Conference., EGPC, Cairo.*, (1998) 236-248.

[15] *USGS*, (2010) 1-4.

[16] Bailey, J., Wallace, M., Larsen, M., Bryant, W., *EGPC 14th Petroleum Conference, Cairo, Egypt*, (1998) 212-221.

[17] Wigger, S., Bailey, J., Larsen, M., Wallace, M., *The Leading Edge*, 16(12) (1997) 1827-1829.

[18] Nashaat M (1998) Abnormally high formation pressure and seal impacts on hydrocarbon accumulations in the Nile Delta and North Sinai basins, Egypt. AAPG Memoir 70: Abnormal Pressures in Hydrocarbon Environments 70:161–180.

[19] Dolson, J.C., Shann, M.V., Matbouly, S.I., Hammouda, H., Rashed, R.M., *GeoArabia-Manama*, 6 (2001) 211-230.

[20] Dewan, J., 1983. Essentials of modern open-hole log interpretation: Pennwell Publ.Co., Tulsa Oklahoma, p. 361.

[21] Tiab, D., Donaldson, E.C., *Gulf professional publishing*, (2015) 224.

[22] Archie, G.E., *Transactions of the AIME*, 146(01) (1942) 54-62.

[23] Pickett, G., *The Log Analyst*, 14 (1973) A1-A21.

[24] Pickett-Heaps, J.D., Northcote, D.H., *Journal of Cell Science*, (1) (1966) 109-120.

[25] Schlumberger, *Well evaluation conference, Egypt*, (1984) 18-26.

[26] Coates, G.R., Dumanoir, J., 1973. A new approach to improved log-derived permeability, SPWLA Annual Logging Symposium. SPWLA, pp. SPWLA--R, p. 27.

[27] Asquith, G.B., Krygowski, D., Gibson, C.R., *Tulsa: American Association of Petroleum Geologists*, 16 (2004) 305-371.

[28] Ghanima, A., Kassab, M.A., Abbas, A., *Egyptian Journal of Petroleum*, 29 (2020) 141-153.

[29] Darling, T., *Elsevier*, (2005) 1-326.

[30] El-Din, E.S., Mesbah, M.A., Kassab, M.A., Mohamed, I.F., Cheadle, B.A., Teama, M.A., *Petroleum exploration and Development*, 40 (2013) 488-494.